



Contents lists available at SciVerse ScienceDirect

Journal of Quantitative Spectroscopy & Radiative Transfer

journal homepage: www.elsevier.com/locate/jqsrt

High sensitivity CW-Cavity Ring Down Spectroscopy of N₂O between 6950 and 7653 cm⁻¹ (1.44–1.31 μm): II. Line intensities



E.V. Karlovets^{a,b}, Y. Lu^{a,c}, D. Mondelain^a, S. Kassı^a, A. Campargue^a, S.A. Tashkun^b, V.I. Perevalov^{b,*}

^a Laboratoire Interdisciplinaire de Physique, CNRS UMR 5588, Université Joseph Fourier de Grenoble B.P. 87, 38402 Saint-Martin-d'Hères Cedex, France

^b Laboratory of Theoretical Spectroscopy, V.E. Zuev Institute of Atmospheric Optics, Siberian Branch, Russian Academy of Sciences, 1, Akademian Zuev Square, 634021 Tomsk, Russian Federation

^c Hefei National Laboratory for Physical Sciences at Microscale, Department of Chemical Physics, University of Science and Technology of China, Hefei 230026, China

ARTICLE INFO

Article history:

Received 27 July 2012

Received in revised form

30 October 2012

Accepted 2 November 2012

Available online 10 November 2012

Keywords:

Nitrous oxide

Infrared spectroscopy

Vibration-rotational transitions

Line intensities

Effective dipole moment parameters

Global treatment

ABSTRACT

The room temperature absorption spectra of nitrous oxide, N₂O, have been recorded in the 6950–7653 cm⁻¹ spectral region at 2 and 10 Torr using a CW-CRDS spectrometer based on 24 fibered DFB lasers. The achieved sensitivity (noise equivalent absorption $\alpha_{min} \approx 5 \times 10^{-11}$ cm⁻¹) allowed detecting lines with intensities as low as 1×10^{-29} cm/molecule. In the preceding contribution (Lu Y, Mondelain D, Liu AW, Perevalov VI, Kassı S, Campargue A, J Quant Spectros and Radiat Transfer 2012;113:749–62), we reported the assignment of more than 7200 N₂O lines in the region and the derivation of the corresponding spectroscopic parameters G_v , B_v , D_v and H_v . In the present work, more than 1300 ¹⁴N₂¹⁶O absolute line intensities of cold and hot bands belonging to the $\Delta P=12, 13$ and 14 series of transitions have been measured ($P=2V_1+V_2+4V_3$ is the polyad number). The uncertainty of the obtained line intensity values varies from 4 to 7% for the majority of the lines. The obtained dataset extends importantly the set of measurements available in the literature, in particular for the $\Delta P=13$ series for which previous data were very limited. The $\Delta P=12-14$ effective dipole moment parameters were fitted to the intensity values measured in this work and available in the literature. The obtained sets of the dipole moment parameters allow reproducing the observed line intensities within their experimental uncertainties. The calculated intensities of the $\Delta P=12, 13$ and 14 bands of ¹⁴N₂¹⁶O assigned by CRDS in the 6950–7653 cm⁻¹ region are provided as supplementary material.

© 2012 Elsevier Ltd. All rights reserved.

1. Introduction

The present contribution continues a series devoted to the study of the near infrared absorption spectrum of nitrous oxide by CW-Cavity Ring Down Spectroscopy (CW-CRDS) [1–5]. Overall, our CRDS studies cover the 5850–7920 cm⁻¹

region corresponding to the spectral range accessible with the set of 80 fibered distributed feedback (DFB) laser diodes used for high sensitivity CW-CRDS in Grenoble. Our previous works were devoted to the assignment and line position analysis of the large set of newly detected transitions. In the present work, we report the derivation and modeling of the line intensities of the main isotopologue, ¹⁴N₂¹⁶O, in the 6950–7653 cm⁻¹ region. The line intensities of the strongest bands of the region were already studied by Fourier Transform spectroscopy (FTS) associated with long multipass

* Corresponding author. Tel.: +7 3822 491794; fax: +7 3822 492086. E-mail address: vip@lts.iao.ru (V.I. Perevalov).

cells [6–8]. But the very high sensitivity of the CRDS technique allowed lowering the detectivity threshold by about three orders of magnitude leading to the observations of many new bands.

The global modeling of the line intensities of $^{14}\text{N}_2^{16}\text{O}$ within the framework of the effective operator method has been performed using the FTS intensity values in a wide wavenumber range [7,9,10]. The region studied in this paper corresponds to transitions belonging to the $\Delta P=12, 13$ and 14 series, where $P=2V_1+V_2+4V_3$ is a polyad number ($V_{i=1-3}$ are the vibrational quantum numbers). In Ref. [7], the eigenfunctions obtained with a previous set of effective Hamiltonian parameters [11] were used for the fitting of the effective dipole moment parameters of these series. We have recently derived an improved set of effective Hamiltonian parameters [12] from a new fit of the measured line positions available in the literature. The corresponding eigenfunctions are used for the intensity calculations of the present work. As a result of the important extension of the experimental dataset and utilization of the eigenfunctions corresponding to the new set of effective Hamiltonian parameters the $\Delta P=12-14$ effective dipole moment parameters are significantly improved, in particular for the $\Delta P=13$ series for which previous intensity measurements were very limited [7].

2. Experiment

For the present intensity retrieval, we use the same spectra as those rovibrationally assigned in Ref. [5]. The N_2O spectra were recorded from 6950 to 7653 cm^{-1} at Doppler limited resolution using CW-Cavity Ring Down Spectrometer based on a series of fibered distributed feedback (DFB) laser diodes [13–15]. The full 6950–7653 cm^{-1} range was covered with the help of twenty four fibered DFB laser diodes, each of them having a typical tuning range of about 35 cm^{-1} by temperature variation from -15 to 60 $^{\circ}\text{C}$. The ring down times ranged between 90 and 220 μs . About 60 min were needed for each DFB laser in order to complete a temperature scan. The ringdown cell (142 cm long) was filled with nitrous oxide in natural isotopic abundance (Air Liquide, Alphagaz, purity $\geq 99.99\%$). The pressure and the ring down cell temperature were monitored during the spectrum recordings. The spectra were obtained at pressure of 10.0 Torr. Additional spectra were recorded at 2.0 Torr in the regions corresponding to the strongest lines, since some of them were too absorptive at 10 Torr.

The wavenumber calibration of the spectra was based on the wavelength values provided by a lambdameter (Burleigh WA-1650). The calibration was further refined using line positions of H_2O present as an impurity in the cell. Their values were taken from the HITRAN database [16]. The typical uncertainty on the line positions is $1 \times 10^{-3} \text{ cm}^{-1}$. A noise equivalent absorption on the order of $\alpha_{\text{min}} \sim 5 \times 10^{-11} \text{ cm}^{-1}$ was achieved. It led to the detection of lines with intensity as small as $1 \times 10^{-29} \text{ cm/molecule}$. The overview of the 10 Torr spectrum in the 7400–7650 cm^{-1} region is presented in Fig. 1. The vibrational labeling of the strongest bands given in this figure is the (P, ℓ_2, r) triplet [5] where P is the polyad number, ℓ_2 the vibrational angular momentum

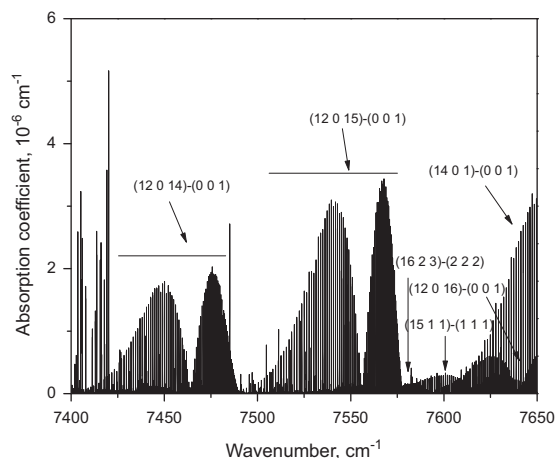


Fig. 1. Overview CW-CRDS spectra of nitrous oxide between 7400 and 7650 cm^{-1} at 294.6 K and 10 Torr. Lines due to water present as an impurity are observed near 7400 cm^{-1} .

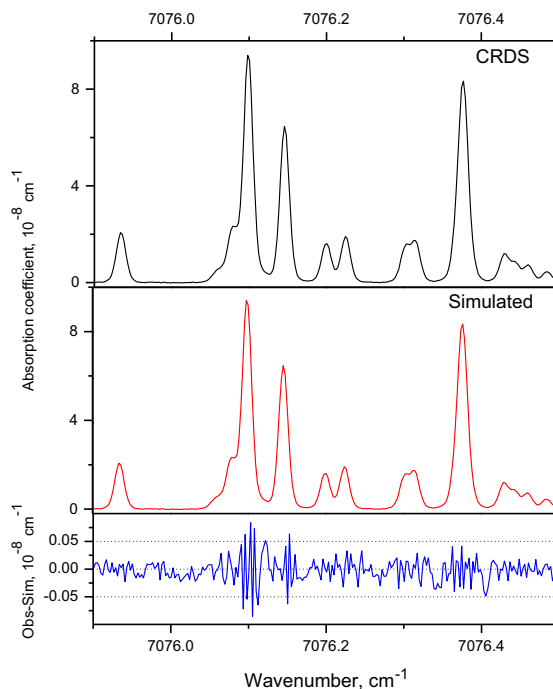


Fig. 2. Comparison of the CRDS spectrum of N_2O near 7076 cm^{-1} to a multiline simulation obtained with a Voigt profile. The spectrum was recorded with a pressure of 10.0 Torr. Residuals are given in lower panel.

quantum number and r is a ranking number within the given (P, ℓ_2) in ascending order

3. Line intensity retrieval

The line intensities were determined using an interactive least-squares multi-line fitting program [17] (<http://fityk.nieto.pl/>), which uses the Levenberg–Marquardt algorithm to minimize the deviation between the observed and calculated spectra. A Voigt profile was adopted as line shape. The Gaussian width was fixed to its theoretical

Doppler value. The integrated line absorbance, line position and Lorentzian width of each line and the corresponding local baseline assumed to be a linear function of the wavenumber, were obtained from this multi-line fitting procedure. An example of line profile fitting is presented in Fig. 2.

The absolute line intensity or integrated absorption coefficient per pressure unit \tilde{S} (in $\text{cm}^{-2} \text{atm}^{-1}$ at temperature T of the spectrum) was deduced from the integrated absorption coefficient I using the equation

$$\tilde{S} = \frac{I}{P}, \quad (1)$$

where P is the N_2O partial pressure (in atm). Each \tilde{S} value was then converted to the absorption line intensity $S(T)$ (in $\text{cm}/\text{molecule}$ at T K) according to the following expression:

$$S(T) = \frac{1}{N_L} \frac{T}{273.15} \tilde{S}, \quad (2)$$

where $N_L = 2.68678 \times 10^{19} \text{ molecule cm}^{-3} \text{atm}^{-1}$ is the Loschmidt number.

In total, 1325 line intensities were retrieved for eight $\Delta P=12$, two $\Delta P=13$ and one $\Delta P=14$ cold bands and two $\Delta P=13$ hot bands. The intensities of the majority of the lines were retrieved from both the 2.0 and 10.0 Torr spectra. The results of the measurements are summarized in Table 1. The experimental uncertainty of the majority of the line intensities is estimated to be between 4% and 7% but for very weak and overlapped lines it reaches 50%. The measured values of the $^{14}\text{N}^{16}\text{O}_2$ line intensities in natural isotopic abundance are provided as Supplementary Material I.

Line intensities of the strongest bands of our region have been reported from spectra recorded by Fourier Transform Spectroscopy (FTS) by Wang et al. [8] and Daumont et al. [7].

Table 1
Summary of the line intensities retrieval.

ΔP	Band ^a	$(P, \ell_2, i)^b$	Band center (cm^{-1})	J_{\max}	N^c	Previous studies
Cold bands						
12	3600-0000	(12 0 9)	7029.843	33	44	
12	4001-0000	(12 0 10)	7137.127	69	130	[7,8]
12	0(12)00-0000	(12 0 11)	7194.365	36	58	
12	3201-0000	(12 0 12)	7214.679	72	105	[7,8]
12	5200-0000	(12 0 13)	7340.792	58	99	[7]
12	6000-0000	(12 0 14)	7463.985	71	126	[7,8]
12	6000-0000	(12 0 15)	7556.135	58	112	[7,8]
12	3600-0000	(12 0 16)	7640.474	56	64	[7]
13	0113-0000	(13 1 1)	7126.979	63	132	[7]
13	2112-0000	(13 1 7)	7443.004	49	38	
14	0203-0000	(14 0 1)	7665.273	72	56	[7,8]
Hot bands						
13	0203-0110	(14 0 1)	7076.507	52	92	
13	0223-0110	(14 2 2)	7084.868	57	198	

^a Assignment according to the maximum value of the modulo of expansion coefficient in the harmonic oscillator basis functions $|V_1 V_2^2 V_3\rangle$.

^b $(P=2V_1+V_2+4V_3, \ell_2, i)$ is a cluster labeling for the upper vibrational state of the band, where P is a polyad number, ℓ_2 is vibrational angular momentum quantum number, and i is the order number within the given values of P and ℓ_2 increasing with the energy.

^c N is the number of lines for which the line intensities were retrieved in this work.

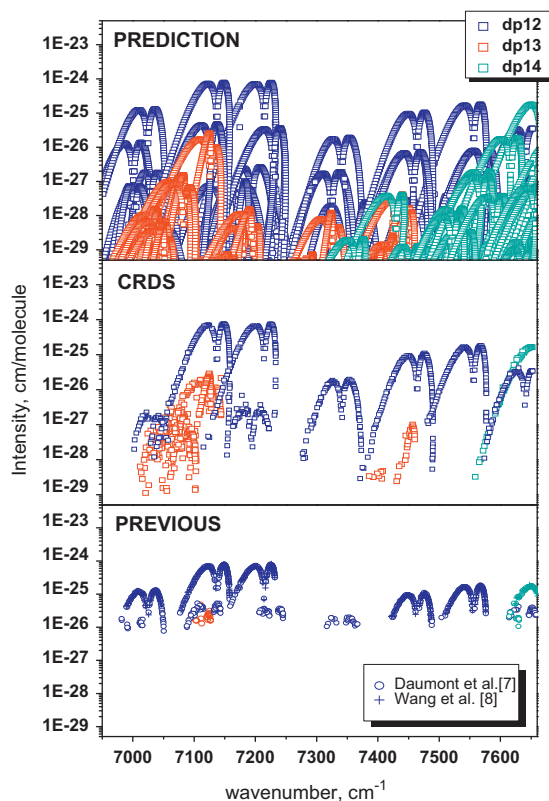


Fig. 3. Overview comparison of the $^{14}\text{N}_2^{16}\text{O}$ line intensities measured in the $6950\text{--}7653 \text{ cm}^{-1}$ region in the present work with the predictions (upper panel) and the observations available in the literature [7,8] (bottom panel). The line intensities are presented for $T=296 \text{ K}$.

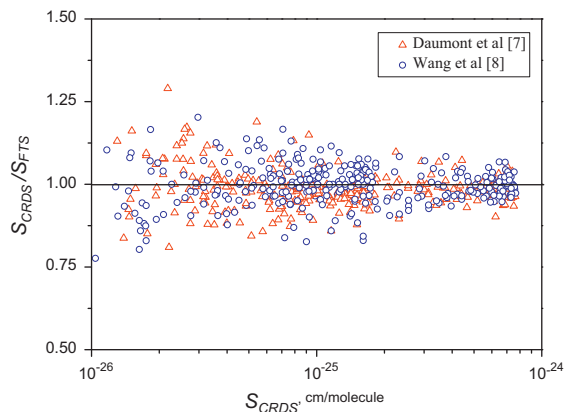


Fig. 4. Ratios of our measured line intensities to those measured by Daumont et al. [7] (open triangles) and by Wang et al. [8] (open circles) for the bands belonging to the $\Delta P=12$ and 14 series of transitions.

The obtained CRDS dataset is compared to the set of previous FTS measurements in Fig. 3. The corresponding CRDS/FTS intensity ratios are displayed in Fig. 4. The overall agreement is reasonable but degrades for the weakest lines (lowest and highest values of the angular momentum quantum number). This results probably from the lack of sensitivity of the FTS measurements leading to larger uncertainties for the weak lines. For instance, in the case of the 0113-0000 band

($\Delta P=13$) only a few line intensities measured with large uncertainties (20–30%) have been reported in Ref. [7]. In the region of the band head of the strong 0003-0000 band the residuals are rather large but they are within the error bars which are also large because of the strong correlations between parameters of the overlapped lines in the inverse problem.

4. Modeling and fitting of the line intensities

The intensity $S_{V'J'\epsilon' \leftarrow VJ\epsilon}$ expressed as cm/molecule at a temperature T of an absorption line corresponding to the transition $V'J'\epsilon' \leftarrow VJ\epsilon$, where V and J are the vibrational index and the angular momentum quantum number, respectively, and $\epsilon = \pm 1$ is the parity, related to the vibrational-rotational transition moment squared $W_{V'J'\epsilon' \leftarrow VJ\epsilon}$ by the well known equation

$$S_{V'J'\epsilon' \leftarrow VJ\epsilon} = \frac{8\pi^3}{3hc} C g_{VJ\epsilon} \frac{\nu_{V'J'\epsilon' \leftarrow VJ\epsilon}}{Q(T)} \exp\left(-\frac{hcE_{VJ\epsilon}}{kT}\right) \left[1 - \exp\left(-\frac{hc\nu_{V'J'\epsilon' \leftarrow VJ\epsilon}}{kT}\right)\right] W_{V'J'\epsilon' \leftarrow VJ\epsilon}, \quad (3)$$

where $E_{VJ\epsilon}$ is the energy of the lower state, $\nu_{V'J'\epsilon' \leftarrow VJ\epsilon}$ is the wavenumber of the transition, $Q(T)$ is the total internal partition function at temperature T , C is the natural isotopic abundance and $g_{VJ\epsilon}$ is the nuclear statistical weight, c is the speed of the light in vacuum and h is Planck constant.

Within the framework of the method of effective operators, the vibrational-rotational transition moment squared is calculated using the eigenfunctions of an effective Hamiltonian [18–20]. In this paper we use eigenfunctions of polyad model of effective Hamiltonian published in our recent paper [12]. The polyad number $P=2V_1+V_2+3V_3$ results from the approximate relations between the three harmonic frequencies

$$\omega_3 \approx 2\omega_1 \approx 4\omega_2. \quad (4)$$

Within the polyad model of effective Hamiltonian the square of the transition dipole moment of a vibration-rotation transition $P'N'J'\epsilon' \leftarrow P N J\epsilon$ is given by [19,20]

$$W_{P'N'J'\epsilon' \leftarrow P N J\epsilon} = (2J+1) \sum_{\substack{2V_1+V_2+4V_3=P \\ \Delta\ell_2=0,\pm 1,\pm 2,\dots}} \sum_{\substack{2\Delta V_1+\Delta V_2+4\Delta V_3=\Delta P \\ \Delta\ell_2=0,\pm 1,\pm 2,\dots}}$$

Table 2

Characteristics of the input data used for the fit of the effective dipole moment parameters.

Series ΔP	Number of lines ^a	Number of bands	J_{\max}	Experimental uncertainty	Reference	RMS (%) ^b
12	118(124)	1	55	5–10%	Toth [6]	5.0
	520(520)	7	48	4–13%	Wang et al. [8]	6.4
	860(914)	16	56	1–50%	Daumont et al. [7]	7.1
	584(658)	8	69	4–7%	This work	5.4
13	18(19)	1	25	10–46%	Daumont et al. [7]	12.7
	412(527)	4	50	4–38%	This work	11.0
14	21(21)	1	33	5%	Toth [6]	10.4
	250(254)	5	46	7–13%	Wang et al. [8]	5.1
	416(467)	10	50	1–50%	Daumont et al. [7]	6.8
	72(93)	1	65	4–7%	This work	5.3

^a Number of fitted line intensities (number of observed line intensities).

^b RMS of fit for a given source.

$$\begin{aligned} & \times J C_{PN\epsilon}^{V_1 V_2 \ell_2 V_3} J' C_{P'N'\epsilon'}^{V_1 + \Delta V_1 V_2 + \Delta V_2 \ell_2 + \Delta \ell_2 V_3 + \Delta V_3} M_{\Delta V}^{|\Delta \ell_2|} \\ & \times \sqrt{f_{\Delta V}^{\Delta \ell_2}(V, \ell_2) \left(1 + \delta_{\ell_2, 0} + \delta_{\ell_2, 0} - 2\delta_{\ell_2, 0} \delta_{\ell_2, 0}\right) \Phi_{\Delta J \Delta \ell_2}(J, \ell_2)} \\ & \times \left(1 + \sum_i \kappa_i^{\Delta V} V_i - \frac{1}{2} \left(b_J^{\Delta V} + 2a_K\right) (2\ell_2 + \Delta \ell_2) \Delta \ell_2 + F_{\Delta V}^{\Delta \ell_2}(J, \ell_2)\right)^2 \end{aligned} \quad (5)$$

Here δ_{ij} is the Kronecker symbol and $J C_{PN\epsilon}^{V_1 V_2 \ell_2 V_3}$ stands for the expansion coefficient determining the eigenfunction

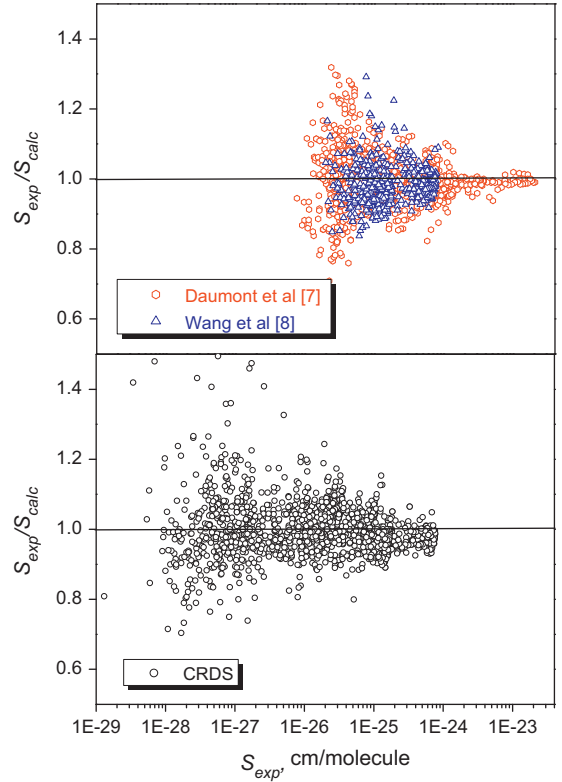


Fig. 5. Ratios of the experimental values of the line intensities from Refs. [7,8] (upper panel) and from this work (lower panel) used to derive the dipole moment parameters to the corresponding calculated values.

Table 3
Effective dipole moment parameters of the $\Delta P=12$ –14 series of transitions of $^{14}\text{N}_2^{16}\text{O}$.

ΔP	ΔV	Δl_2	$M(D)^a$		K_2		b_j		d_j (or a_K) ^b		χ	RMS (%)
			This work	Ref. [7]	This work	Ref. [7]	This work	Ref. [7]	This work	Ref. [7]		
12	0	0	3	0	$2.964(3) \times 10^{-4}$	$2.989(7) \times 10^{-4}$	$2.5(3) \times 10^{-2}$	$2.8(6) \times 10^{-2}$	$-3.3(3) \times 10^{-4}$	$-3.5(7) \times 10^{-4}$	0.9	6.4
	2	0	2	0	$-1.7(2) \times 10^{-6}$	$-9(2) \times 10^{-6}$						
	1	2	2	0	$4.24(1) \times 10^{-5}$	$3.5(2) \times 10^{-5}$						
	4	0	1	0	$2.756(3) \times 10^{-5}$	$3.12(2) \times 10^{-5}$						
	3	2	1	0	$1.47(4) \times 10^{-6}$	$-4(2) \times 10^{-7}$			$-4.6(7) \times 10^{-3}$	$4(3) \times 10^{-2}$		
	2	4	1	0	$-5.7(2) \times 10^{-7}$	$-2.9(7) \times 10^{-7}$			$2(1) \times 10^{-2}$			
	6	0	0	0	$4.977(3) \times 10^{-6}$	$4.01(3) \times 10^{-6}$						
	5	2	0	0	$-6.85(3) \times 10^{-7}$	$-9.3(6) \times 10^{-7}$						
	4	4	0	0	$2.3(2) \times 10^{-8}$	$1.3(4) \times 10^{-7}$						
	3	6	0	0	$-5.29(6) \times 10^{-8}$							
2	8	0	0	$-1.22(1) \times 10^{-8}$								
1	10	0	0	$-0.99(1) \times 10^{-9}$								
13	0	1	3	1	$6.25(2) \times 10^{-6}$	$6.6(3) \times 10^{-6}$	$2.3(5) \times 10^{-2}$		$-1.23(1) \times 10^{-2}$	$-1.2(9) \times 10^{-2}$	1.6	11
	2	1	2	1	$2.69(6) \times 10^{-6}$				$1.96(1) \times 10^{-2}$			
14	1	0	3	0	$1.154(1) \times 10^{-4}$	$1.129(2) \times 10^{-4}$	$1.8(5) \times 10^{-2}$	$2(1) \times 10^{-2}$			0.7	6.3
	0	2	3	0	$-6.23(2) \times 10^{-6}$	$-5.70(7) \times 10^{-6}$						
	3	0	2	0	$-1.521(5) \times 10^{-5}$	$-2.11(1) \times 10^{-5}$						
	2	2	2	0	$2.3(9) \times 10^{-7}$	$-3.4(2) \times 10^{-6}$				$5(3) \times 10^{-6}$		
	1	4	2	0	$1.2(4) \times 10^{-7}$	$-2.9(8) \times 10^{-7}$						
	5	0	1	0	$3.14(2) \times 10^{-6}$	$3.28(7) \times 10^{-6}$						

^a All the parameters values are in Debye, except for K_2 , b_j , d_j , and a_K , which are dimensionless.

^b The values of d_j parameter are presented for $\Delta P=12$ and 14 series of transitions but for $\Delta P=13$ series the value of parameter a_K is given.

^c The values between parentheses represent three standard deviations in the units of the last digit quoted.

of the lower state

$$\Psi_{PNJ\epsilon}^{\text{eff}} = \sum_{\substack{2V_1 + V_2 + 4V_3 = P \\ \ell_2}} J C_{PN\epsilon}^{V_1 V_2 \ell_2 V_3} |V_1 V_2 | \ell_2 | V_3 J \epsilon \rangle \quad (6)$$

The summation runs over all states within the polyad involved. The definition of the Wang-type basis functions $|V_1 V_2 | \ell_2 | V_3 J \epsilon \rangle$ is given, for example, in Ref. [19]. In the same way, $J C_{PN\epsilon}^{V_1 V_2 \ell_2 V_3}$ stands for the expansion coefficient within the upper-state polyad. The functions $\Phi_{\Delta J \Delta \ell_2}(J, \ell_2)$ for $\Delta \ell_2 = 0, \pm 1$ are equal to the Clebsch–Gordan coefficients $(1 \Delta \ell_2 J \ell_2 | J + \Delta J) (\ell_2 + \Delta \ell_2)$, related to the Hönl–London factors by the equation

$$|(1 \Delta \ell_2 J \ell_2 | J + \Delta J) (\ell_2 + \Delta \ell_2)|^2 = \frac{L_{\Delta J}^{\Delta \ell_2}}{2J + 1}. \quad (7)$$

The $f_{\Delta V}^{\Delta \ell_2}(V, \ell_2)$ functions are listed in Table 1 of Ref. [21] for small values of the quantum number differences ΔV . The Herman–Wallis-type functions $F_{\Delta V}^{\Delta \ell_2}(J, \ell_2)$ appearing in Eq. (5) are given in Ref. [22]. Here, only the two first terms were used

$$F_{\Delta J \Delta \ell_2}^{\Delta V}(J, \ell_2) = b_J^{\Delta V} m + d_J^{\Delta V} m^2 \quad (8)$$

for $\Delta \ell_2 = 0, \pm 1$ matrix elements with $m = -J, J + 1$ for P - and R -branches, respectively. The parameters of the matrix elements of the effective dipole moment operator $M_{\Delta V}^{|\Delta \ell_2|}$, $\kappa_i^{\Delta V}$ ($i = 1, 2, 3$), $a_K^{\Delta V}$, $b_J^{\Delta V}$, $d_J^{\Delta V}$ are determined by least squares fitting to the observed line intensities.

The line intensities from this work and those from Daumont et al. [7], Wang et al. [8] and Toth [6] were used to fit the effective dipole moment parameters of the $\Delta P = 12, 13$ and 14 series of bands. The characteristics of the input data are given in Table 2. The intensity values were weighted according to their uncertainties included in Table 2. In Ref. [7], the uncertainties of the individual lines are provided. In Ref. [6] for different lines two uncertainties are given: 5% and 10%. In Ref. [8], three gradations of the accuracy of the line intensities are given: uncertainties are 5% for well-isolated lines, 7% for the majority of the lines and 13% for very weak or overlapped lines. For our measurements we also used three gradations for the uncertainty values: 4% for well-isolated lines, 5% for the majority of the lines and 7% for very weak lines. In the case of the $\Delta P = 13$ bands, we attached an uncertainty value to each line because the majority of these lines are weak or blended. As a rule, strongly overlapped lines and lines with uncertainties larger than 38% were excluded from the fits.

The partition function from Ref. [23] was used in all fits.

The weighted standard deviation of the fits, χ , of the $\Delta P = 12$ and 14 series does not exceed 1.0 indicating that the obtained sets of effective dipole moment parameters reproduce the measured line intensities within their experimental uncertainties. The overall agreement is illustrated in Fig. 5 where the ratios of the experimental and fitted values of the line intensities are displayed. In the case of the $\Delta P = 13$ series, we obtained $\chi = 1.6$ which may indicate that the experimental uncertainties of these weak lines have been underestimated.

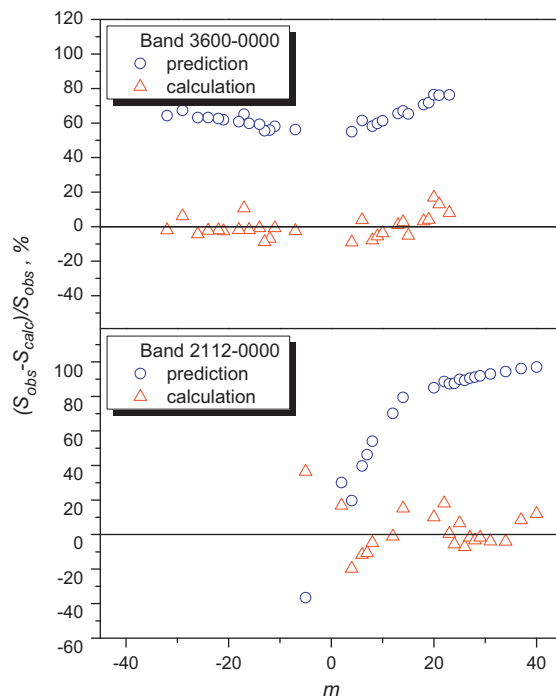


Fig. 6. Comparison of the CRDS intensity values to the line intensities predicted with the previous set of the effective dipole moment parameters [7] (open circles) and calculated with the new set of the parameters (open triangles). Upper panel: 3600-0000 band ($\Delta P = 12$) centered at 7029.843 cm^{-1} . Lower panel: 2112-0000 band ($\Delta P = 13$) centered at 7443.004 cm^{-1} . The experimental uncertainty of the line intensities for the 3600-0000 band is about 5% and that for the 2112-0000 band varies from 30% (small m values) to 7% for the majority of lines.

In Table 3, the fitted sets of the effective dipole moment parameters are presented and compared to their previous determination by Daumont et al. [7]. A good agreement is noted for the effective dipole moment parameters which are responsible for the line intensities of the strongest bands but most of the Herman–Wallis coefficients differ considerably in value and even in sign. This is mainly due to the fact that the eigenfunctions used in Ref. [7] for the intensity calculations were obtained with our previous set of effective Hamiltonian parameters [11]. But since 1999, a lot of new measurements of $^{14}\text{N}_2^{16}\text{O}$ line positions were published, in particular from our CRDS studies in the $5800\text{--}7900 \text{ cm}^{-1}$ region [1–5]. Because of the high sensitivity, these CRDS measurements involved very weak bands and hot bands reaching highly excited vibrational states up to $10,000 \text{ cm}^{-1}$. We have recently performed a new fit of the effective Hamiltonian parameters [12] based of the exhaustive review of the published data. The eigenfunctions corresponding to the new set of effective Hamiltonian parameters were used in the present work for the intensity calculations. The second reason of the differences in the obtained effective dipole moment parameters is that the input dataset was considerably enlarged in the present fit by adding intensity values of five new bands and many new high J transitions of the others (see Table 2). In addition, line intensities from Ref. [8] were not used in Ref. [7] but are included in the present fit.

5. Conclusion

New CRDS measurements of $^{14}\text{N}_2^{16}\text{O}$ line intensities in the 6950–7653 cm^{-1} region and improved eigenfunctions [12] have allowed to derive an improved set of effective dipole parameters for the $\Delta P=12$, 13 and 14 series of transitions. The improvement is particularly important for the $\Delta P=13$ series of transitions because only few line intensities for the strongest 0113-0000 band of this series were available with very large uncertainties [7].

As an illustration of the achieved gain, we compare in Fig. 6, the intensities of two bands 3600-0000 ($\Delta P=12$) and 2112-0000 ($\Delta P=13$) centered at 7029.843 and 7443.004 cm^{-1} , respectively, to the corresponding intensity values predicted with the previous set of the effective dipole moment parameters [7]. The residuals reach 100% while the experimental values are satisfactorily reproduced with the new set of parameters.

In order to provide complete information for $^{14}\text{N}_2^{16}\text{O}$ in the 6950–7653 cm^{-1} range, we provide as [Supplementary Material](#), calculated position and line intensities for the whole set of $^{14}\text{N}_2^{16}\text{O}$ bands reported in Ref. [5]. The line intensities are calculated with the help of the eigenfunctions of the effective Hamiltonian from Ref. [12] and the effective dipole moment parameters obtained in this work.

Acknowledgments

This work is jointly supported by RFBR (Russia, grant no 12-05-93106) and CNRS (France) in the frame of Groupe-ment de Recherche International SAMIA (Spectroscopie d'Absorption des Molécules d'Intérêt Atmosphérique).

Appendix A. Supplementary data

Supplementary data associated with this article can be found in the online version at <http://dx.doi.org/10.1016/j.jqsrt.2012.11.003>.

References

- [1] Liu AW, Kassı S, Malara P, Romanini D, Perevalov VI, Tashkun SA, et al. High sensitivity CW-cavity ring down spectroscopy of N_2O near 1.51 μm (I). *J Mol Spectrosc* 2007;244:33–47.
- [2] Liu AW, Kassı S, Perevalov VI, Tashkun SA, Campargue A. High sensitivity CW-cavity ring down spectroscopy of N_2O near 1.51 μm (II). *J Mol Spectrosc* 2007;244:48–62.
- [3] Liu AW, Kassı S, Perevalov VI, Hu SM, Campargue A. High sensitivity CW-cavity ring down spectroscopy of N_2O near 1.5 μm (III). *J Mol Spectrosc* 2009;254:20–7.
- [4] Liu AW, Kassı S, Perevalov VI, Tashkun SA, Campargue A. High sensitivity CW-cavity ring down spectroscopy of N_2O near 1.28 μm . *J Mol Spectrosc* 2011;267:191–9.
- [5] Lu Y, Mondelain D, Liu AW, Perevalov VI, Kassı S, Campargue A. High sensitivity CW-cavity ring down spectroscopy of N_2O between 6950 and 7653 cm^{-1} (1.44–1.31 μm): I. Line positions. *J Quant Spectrosc Radiat Transfer* 2012;113:749–62.
- [6] Toth RA. Line positions and strengths of N_2O between 3515 and 7800 cm^{-1} . *J Mol Spectrosc* 1999;197:158–87.
- [7] Daumont L, Vander Auwera J, Teffo JL, Perevalov VI, Tashkun SA. Line intensity measurements in $^{14}\text{N}_2^{16}\text{O}$ and their treatment using the effective dipole moment approach. II. The 5400–11,000 cm^{-1} region. *J Quant Spectrosc Radiat Transfer* 2007;104:342–56.
- [8] Wang L, Perevalov VI, Tashkun SA, Gao B, Hao LY, Hu SM. Fourier transform spectroscopy of N_2O weak overtone transitions in the 1–2 μm region. *J Mol Spectrosc* 2006;237:129–36.
- [9] Daumont L, Vander Auwera J, Teffo JL, Perevalov VI, Tashkun SA. Line intensity measurements in $^{14}\text{N}_2^{16}\text{O}$ and their treatment using the effective dipole moment approach: I. The 4300–5200 cm^{-1} region. *J Mol Spectrosc* 2001;208:281–91.
- [10] Daumont L, Claveau C, Debacker-Barilly MR, Hamdouni A, Régalia-Jarlot L, Teffo JL, et al. Line intensities of $^{14}\text{N}_2^{16}\text{O}$: the 10 μm region revisited. *J Quant Spectrosc Radiat Transfer* 2002;72:37–55.
- [11] Perevalov VI, Tashkun SA, Teffo JL. Global fitting of rovibrational line positions of nitrous oxide. Sixteenth Colloquium on High Resolution Molecular Spectroscopy, Dijon (France). 6–10 Sept. 1999, Poster D2, p. 103.
- [12] Perevalov VI, Tashkun SA, Kochanov RV, Liu AW, Campargue A. Global modeling of the $^{14}\text{N}_2^{16}\text{O}$ line positions within the framework of the polyad model of effective Hamiltonian. *J Quant Spectrosc Radiat Transfer* 2012;113:1004–12.
- [13] Macko P, Romanini D, Mikhailenko SN, Naumenko OV, Kassı S, Jenouvrier A, et al. High sensitivity CW-cavity ring down spectroscopy of water in the 1.5 μm atmospheric window. *J Mol Spectrosc* 2004;227:90–108.
- [14] Morville J, Romanini D, Kachanov AA, Chenevier M. Two schemes for trace detection using cavity ringdown spectroscopy. *Appl Phys* 2004;D78:465–76.
- [15] Perevalov BV, Kassı S, Romanini D, Perevalov VI, Tashkun SA, Campargue A. CW-cavity ringdown spectroscopy of carbon dioxide isotopologues near 1.5 μm . *J Mol Spectrosc* 2006;238:241–55.
- [16] Rothman LS, Gordon IE, Barbe A, Chris Benner D, Bernath PF, Birk M, et al. The HITRAN 2008 molecular spectroscopic database. *J Quant Spectrosc Radiat Transfer* 2009;110:533–72.
- [17] Wojdyr M. Fityk: a general-purpose peak fitting program. *J Appl Cryst* 2010;43:1126–8.
- [18] Teffo JL, Perevalov VI, Lyulin OM. Reduced effective Hamiltonian for a global treatment of rovibrational energy levels of nitrous oxide. *J Mol Spectrosc* 1994;168:390–403.
- [19] Lyulin OM, Perevalov VI, Teffo JL. Effective dipole moment and band intensities of nitrous oxide. *J Mol Spectrosc* 1995;174:566–80.
- [20] Lyulin OM, Perevalov VI, Teffo JL. Fitting of line intensities using the effective operator approach: The 4 μm Region of $^{14}\text{N}_2^{16}\text{O}$. *J Mol Spectrosc* 1996;180:72–4.
- [21] Perevalov VI, Lobodenko EI, Lyulin OM, Teffo JL. Effective dipole moment and band intensities problem for carbon dioxide. *J Mol Spectrosc* 1995;171:435–52.
- [22] Teffo JL, Lyulin OM, Perevalov VI, Lobodenko EI. Application of the effective operator approach to the calculation of $^{13}\text{C}^{16}\text{O}_2$ line intensities. *J Mol Spectrosc* 1998;187:28–41.
- [23] Fischer J, Gamache RR, Goldman A, Rothman LS, Perrin A. Total internal partition sums for molecular species in the 2000 edition of the HITRAN database. *J Quant Spectrosc Radiat Transfer* 2003;82:401–12.